Optics Communications 284 (2011) 1435–1438

Contents lists available at ScienceDirect

Optics Communications

journal homepage: www.elsevier.com/locate/optcom

Sensor with increased sensitivity based on enhanced optical transmission in the infrared

Olga Krasnykov, Alina Karabchevsky, Atef Shalabney, Mark Auslender, I. Abdulhalim *

Department of Electrooptic Engineering, Ben Gurion University of the Negev, Beer Sheva 84105, Israel

ARTICLE INFO

Article history:
Received 6 April 2010
Received in revised form 5 June 2010
Accepted 22 October 2010

ABSTRACT

Using enhanced optical transmission (EOT) through periodic nanoslits in thin metal films we demonstrate sensing in water with highly enhanced sensitivity in the infrared range for the first time. This is explained as a result of the enhancement in the penetration depth in the analyte thus increasing the interaction volume which in turn increases the sensitivity and allows for sensing of large bio-entities. The penetration depth enhancement in the EOT case is found to be larger than the corresponding enhancement factor in the Kretschmann configuration.

Introduction

Refractive index sensors with large sensitivity are desirable for many applications to be able to detect minute levels (less than picograms) of pollutants. [1] Such sensors are of high importance for protection from dangerous threats of toxic materials and dangerous viruses. One of the heavily investigated types of optical sensing mechanisms these days is based on enhanced optical transmission (EOT) through nanoapertured metallic thin films. These structures are planar and operating at normal incidence, thus the possibility of producing and operating them in large arrays to provide what is called a biochip. The EOT phenomenon is related to the excitation of surface plasmon resonances (SPRs) excited at the surface of the nanoapertures, [2,3] The sensing mechanism is based on the existence of evanescent field inside the analyte which is affected by the variation of the refractive index of the analyte. Hence the sensitivity depends on the strength of this field and on its extent within the analyte called the penetration depth. Since with SPR phenomena the field is enhanced in the nm vicinity of the metal dielectric interface, the sensitivity of localized SPR based sensors has been shown recently [4] to exceed that of extended SPR sensors when the index variations are occurring only in the nm vicinity of the nanofeature. To detect bulk variations in the analyte and pollutants with few microns size such as bacteria, the deep penetration of the field in the analyte is important. In the visible range of the spectrum the enhanced local field extends only to a range of about 50–100 nm inside the analyte; hence it will not sense the whole volume of a bacteria cell for example. This problem is well known in the traditional prism coupled SPR sensors even though extended SP waves have a relatively larger propagation length along the surface of the order of 1 μm. [5] Long range SPR configurations were proposed [6] to resolve this problem. The interest in SPR sensing using prism coupling to continuous metal film so called standard Kretschmann configuration for sensing in the IR range was raised recently [7] since many biomolecules have specific absorption bands in the IR range, thus performing multi wavelength SPR measurements allow these biomolecules to be identified selectively. Sensors based on EOT, strongly depend on the detailed structure of the nanomaterial. It is well known that the aperture size and type of the metallic nanostructures have different contributions to the extraordinary transmission, [8–11] Observation of the EOT phenomenon in the mid infrared was achieved [12] by using doped InSb as the patterned material and even in the THz region [13] but none of these works were devoted to sensing application. Our proposed structure designed for the infrared both enhances the sensitivity and overcomes the problem of detecting large biological entities by extending the penetration depth of the electromagnetic field inside the analyte. It is found that the penetration depth in the IR for the EOT case is larger than that for the SPR case in Kretschmann configuration.

To describe the concept we focus on the case of a one dimensional (1D) periodic array of nanoslits, although the same idea applies to other periodic structures in metals such as a 2D array of nanoholes. Fig. 1a shows the general 1D structure and the geometrical parameters. When the nanoslits structure is irradiated by TM polarized light at normal incidence one obtains resonant transmission peaks as shown in Fig. 1b. The resonance wavelength is found from the k vector matching condition of SPR existence, $k_x = k_{sp}$:

$$\lambda_{SP} \approx \mathrm{Re}\left\{\Lambda\sqrt{\frac{\varepsilon_m \varepsilon_a}{\varepsilon_m + \varepsilon_a}}\right\} \quad (1)$$

where $\varepsilon_m = \varepsilon_{mr} + i\varepsilon_{mi}$ is the metal dielectric constant and ε_a is the dielectric constant of the analyte. Eq. (1) is valid for the 1st resonance

* Corresponding author.
E-mail address: abdulhlm@bgu.ac.il (I. Abdulhalim).

0030-4018/$ – see front matter © 2010 Elsevier B.V. All rights reserved.
doi:10.1016/j.optcom.2010.10.076

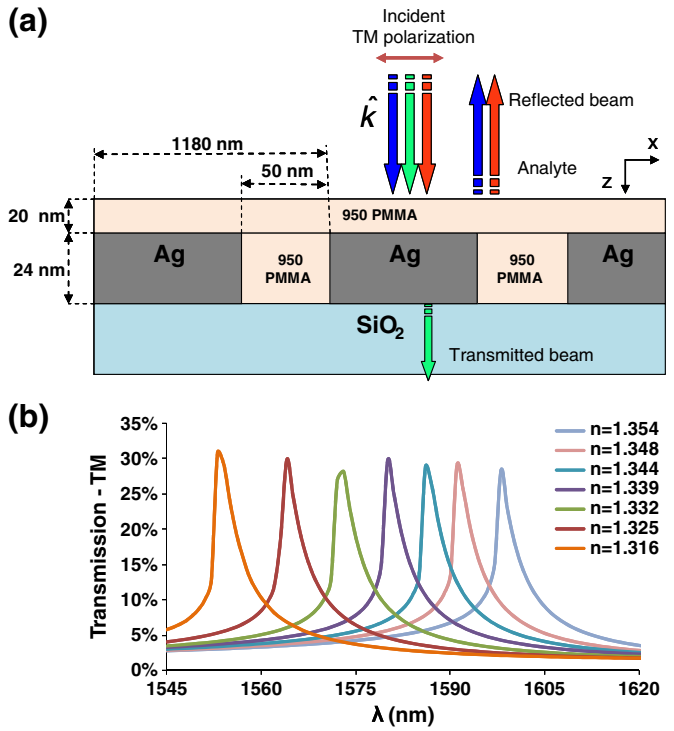

Fig. 1. (a) The design of sensor for IR range and (b) simulated EOT spectra through this structure at different analyte refractive indices in the range 1.316–1.354. The analyte is on top of the PMMA layer.

peak and for thick metal film, however it is used as well for estimating the SPR location for thin metal films as the thickness of the metal film has small effect on the *k*-vector of the plasmon. [14] In our earlier publication [15] we have compared this equation with the rigorous calculations and found very good agreement, although not perfect, but for the purposes of designing a sensor it is adequate. It should also be mentioned that for perforated films the accuracy of Eq. (1) depends on the space width between two metallic lines. The smaller the space is the better the accuracy, as we have checked that with the rigorous calculations. The sensitivity of the sensor is measured in nm per refractive index units (nm/RIU) defined [16] as the slope of the variation λ_{SP} with the analyte index $n_a = \sqrt{\varepsilon_a}$ and can be derived from Eq. (1):

$$S = \frac{\lambda_{SP}}{\sqrt{\varepsilon_a}} \frac{\varepsilon_{mr}}{\varepsilon_{mr} + \varepsilon_a - 0.5\varepsilon_{mr}^{-1}\varepsilon_a\lambda_{SP}\frac{\partial\varepsilon_{mr}}{\partial\lambda}} \tag{2}$$

Hence only when the metal dispersion is ignored the sensitivity scales linearly with the structure period Λ and the wavelength. Since usually in the IR $|\varepsilon_{mr}| >> \varepsilon_a$, Eq. (2) leads to $S_\lambda \approx \lambda_{SP}/n_a$. Another important factor related to the sensitivity is the penetration depth of the electromagnetic field inside the analyte which from the SPR theory in Kretschmann configuration it can be estimated from the following equation:

$$\delta_a = \frac{\lambda}{2\pi}\cdot\sqrt{\frac{\varepsilon_a + \varepsilon_{mr}}{-\varepsilon_a^2}} \tag{3}$$

For example for silver at $\lambda = 1550$ nm we have $\varepsilon_{mr} = -115.5$ which is much larger than $\varepsilon_a = 1.769$, thus giving a penetration depth of about $\delta_a = 0.96\lambda \approx 1.48$ μm. For the visible range $\lambda = 600$ nm on the other hand we have $\varepsilon_{mr} = -14.14$, thus giving $\delta_a = 0.316\lambda \approx 0.19$ μm. Hence the penetration depth in the near IR (NIR) range is larger by a factor of 8 than that in the visible range, although the wavelength ratio is only 2.5. The reason for that is the difference in the real part of the metal dielectric function. In addition to the linear scaling of the sensitivity with the wavelength, another important concept of this paper is that the EOT structure can be designed such that the penetration depth in the analyte is increased much more than Eq. (3) predicts in contrary to the case of SPs in the standard Kretschmann configuration [17] as will be shown below based on the field calculations. The reason for this behavior is unclear for the moment but apparently perforated films offer a greater range of parameter tuning that allows achieving higher penetration depth.

In order to help verify this concept we have first performed simulations of EOT phenomenon and its dependence on the grating parameters. The structure as shown in Fig. 1a is a result of optimization for the wavelength range 1500 nm–1600 nm in terms of maximum transmittance and the stability of the silver obtained by the PMMA cover layer. Investigation of gratings that gave EOT resonance in the visible range was published by us recently [15,18] while here we concentrate on the enhanced sensitivity obtained in the IR range. Fig. 1b simulated EOT spectra through this structure at different analyte refractive indices in the range 1.33–1.35 showing sensitivity of about 1200 nm/RIU. By increasing the pitch of the grating, the sensitivity of the sensor and the resonance wavelength increases linearly with the pitch as one can easily see from Fig. 2. At each wavelength one has to optimize the width and height of the gratings to get the maximum peak height, but these parameters do not influence the sensitivity. Although in the long wave IR, silver film thicknesses with $h<5$ nm were used, they are impractical since they are usually nonuniform and their response is different from that of the bulk. We have used them here to show that in principle the sensitivity continues to scale linearly with the pitch even for such large pitches. Other types of metals might be more suitable for the long wavelength range of the IR.

The optimum design as shown in Fig. 1a was fabricated at BGU nanofabrication facility. The fabrication involves deposition of the metal layer and electron beam lithography for nanostructure patterning. The Ag was deposited on a silica substrate using electron gun system with deposition rate of 0.6 Å/s. After Ag deposition a thin layer of PMMA was spun, and baked for 3 min at 180 °C. The electron

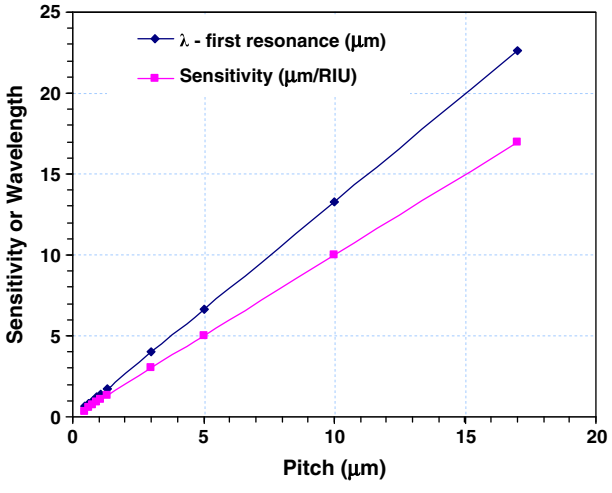

Fig. 2. Rigorous coupled wave analysis (RCWA) simulations results: the blue dots represent the sensitivity versus grating period; the pink squares represent the location of the first resonance. The structure is similar to Fig. 1a but the values for the space width *W* and metal thickness *h* were varied to obtain maximum peak height as follows: (1) for pitches in the range $\Lambda = 450$ nm − 3000 nm: $W = 45$ nm, $h = 45$ nm, (2) for $\Lambda = 5000$ nm, 10,000 nm, 17,000 nm the width is $W = 100$ nm while the thickness has to be reduced to $h = 5$ nm, 1 nm, 0.5 nm respectively. The PMMA layer thickness is 20 nm for all pitches up to 5000 nm while it was reduced to 5 nm for pitches of 10,000 nm and 17,000 nm.

beam writing, done by e-line system of Raith at 20 keV and low current. The system writes 2 mm line long without stitching using FBMS (Fix Beam Moving Stage) mode. After writing we develop the PMMA using MIBK: IPA 1:3 for 45 s at 22 °C. For etching the Ag lines the PMMA is used as a mask and we etch by ion beam milling for 4 min. The last stage of sensor fabrication included spinning of the PMMA (<15 nm thickness) on Ag grating surface for encapsulation. To characterize the structure a polarized reflection–transmission setup was built as shown in Fig. 3. The light source is a fiber coupled tunable laser operating in the range 1500–1620 nm. The light output at the distal end of the fiber is collimated with a microscope objective lens, passing through a polarizer and through a pinhole of the same size as the sample and a beam splitter. The sample is held on an x–y rotating stage to allow best alignment to the beam and the polarizer. Analytes were dripped and pumped by digital micropipette. The transmitted beam was collected with a lens similar to the collimation lens and focused to an InGaAs detector. Transmission signals from the detector were digitized with a digital oscilloscope, transferred to a personal computer and processed with Matlab in real time. The refractive-index sensitivity of the designed structure as a sensor was investigated using the organic analyte: ethanol in de-ionized (DI) water because such mixtures have known refractive indices. DI water served as the reference.

Fig. 4a shows experimental EOT spectra measured at different concentrations of ethanol in water. Note that the peak height increases as the ethanol concentration increases. This was confirmed by the simulations to be a result of the absorption of DI water at these wavelengths which decreases when more and more ethanol is present. A quantitative comparison between the rigorous and

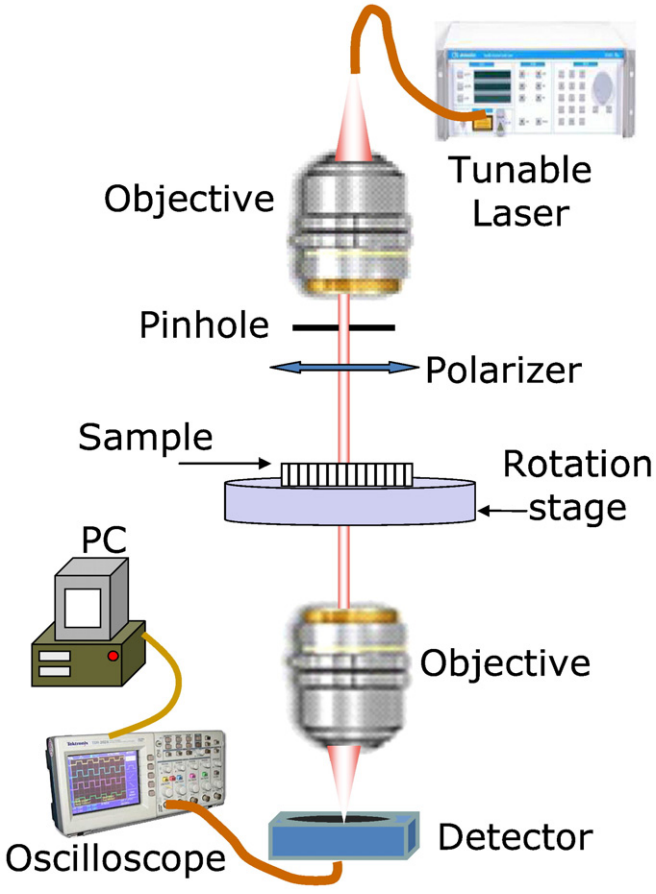

Fig. 3. The experimental setup.

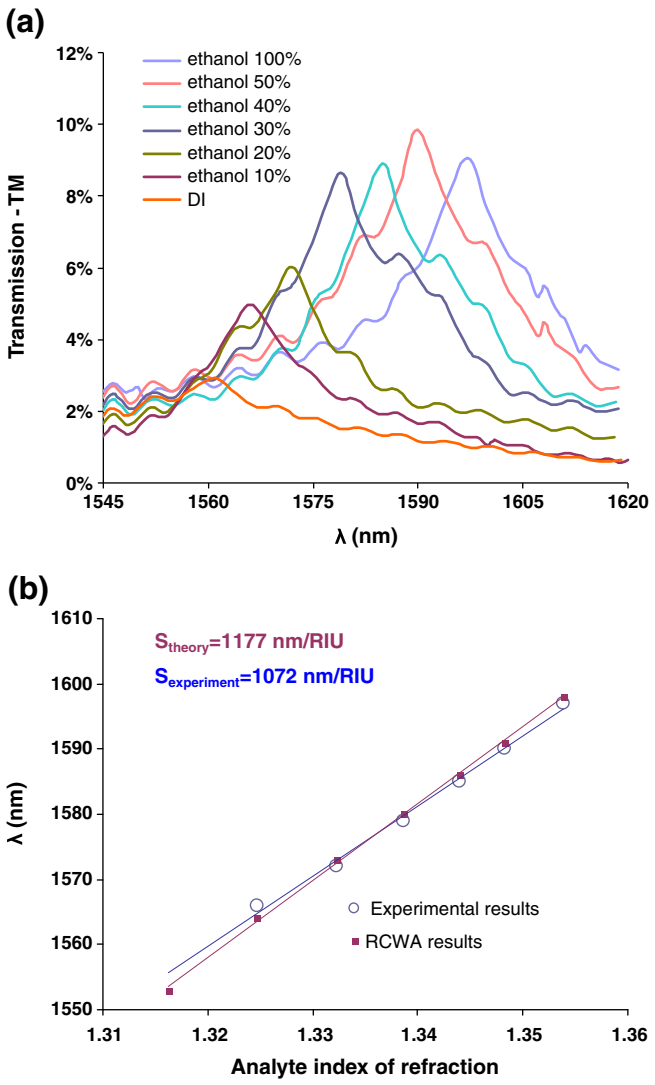

Fig. 4. (a) Experimental EOT spectra measured at different concentrations of ethanol in water; (b) the experimental and theoretical sensitivities.

experimental peak heights show a difference of about 20% which can be due to slight variations in the gratings parameters from the design, however this comparison is not of interest here as for the sensor functionality the peak location is the most important. In order to decrease the water absorption, the pathlength of the beam inside the analyte can be reduced further. In our case it was 3 mm, but in a practical sensor design one can build a cavity of only 0.1 mm gap and let the analyte flow through it. The experimental and theoretical sensitivities are shown in Fig. 4b demonstrating excellent agreement. Based on the fact that the tunable laser used has a resolution of $\langle\delta\lambda\rangle = 1pm$, the detection limit of our system is $\langle\delta n\rangle = \langle\delta\lambda\rangle/S_\lambda \approx 10^{-6} RIU$.

In order to show that the penetration depth indeed increases in the IR range for the EOT sensor, we calculated the evanescent field and the energy distribution at first resonance wavelength within the analyte for the structure that was designed for the visible range and was presented in our earlier works [15,16] and for the structure that is presented here. Fig. 5a and b show the energy distribution in the analyte: $U(x,z) = |E_x|^2 + |E_z|^2$ both for the visible design and the NIR designs respectively. If we compare the field distributions, and assuming an exponential decay we estimated the penetration depth as the distance inside the analyte when the field decays to $1/e$ of its maximum value. We get that the penetration depth for the NIR design

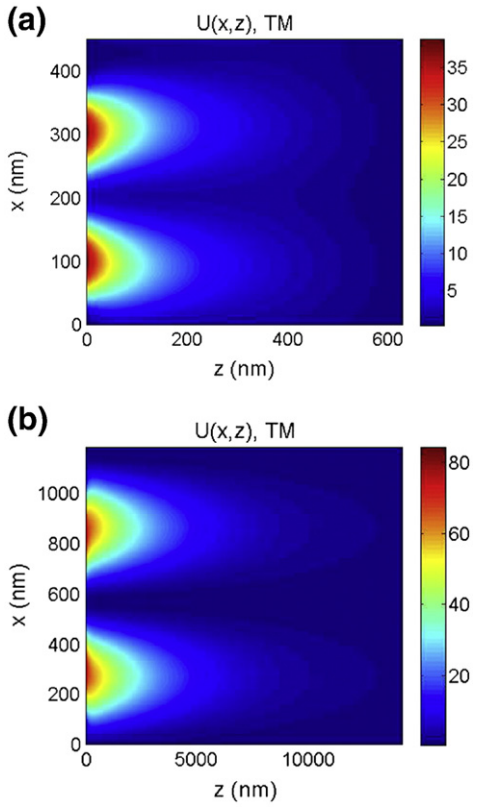

Fig. 5. (a) Distribution of the electric energy density of the silver grating on SiO_2 substrate and PMMA cover where the grating period is 450 nm, slit width is 45 nm, grating height is 45 nm, cover height is 15 nm, the refractive index of analyte is 1.34 and the wavelength is 629 nm; (b) distribution of the electric energy density of the silver grating on SiO_2 substrate and PMMA cover where the grating period is 1180 nm, height is 24 nm, slit width is 50 nm cover height is 20 nm, the refractive index of analyte is 1.34 and the wavelength is 1582 nm.

is around 5.17 μm which is 22 times larger than the penetration depth for visible range sensor. This is larger than the penetration depth predicted by Eq. (3). In addition we calculated the energy density per unit area by integration over the whole interaction volume in the analyte according to:

$$u = \frac{1}{\Lambda Z_{max}} \int_{x=0}^{\Lambda} \int_{z=0}^{Z_{max}} U(x,z)dxdz \quad (5)$$

We consider the first resonance wavelength (λ_{res}) as Z_{max} for visible range, and $9\lambda_{res}$ as Z_{max} for NIR range. The ratio between the energy density per area unit in NIR range and visible range is equal to 1.7. The increase in the energy density is one of the reasons for sensitivity enlargement in the IR range.

To conclude, we have demonstrated enhanced refractive index sensing in the infrared using the enhanced resonant transmission phenomenon in metallic nanoslit arrays. The penetration depth in the IR in the EOT case was found to be larger than that for extended SPs in the standard Kretschmann configuration thus compensating for the loss in the propagation length or the interaction volume. This IR sensor will have applications for biomolecules SPR spectroscopy and the detection of large biological entities such as cells.

Acknowledgements

This research is supported by the Ministry of Science under Tashtiot program. We are grateful to Benny Hadad and Adi Gold from The Weiss Family Laboratory for Nanoscale Systems at BGU for their help during the fabrication of the nanostructure.

References

[1] I. Abdulhalim, M. Zourob, A. Lakhtakia, in: R.S. Marks, C.R. Lowe, D.C. Cullen, H.H. Weetall, I. Karube (Eds.), The Handbook of Biosensing and Biochips, Wiley, 2007.
[2] S.A. Kalele, N.R. Tiwari, S.W. Gosavi, S.K. Kulkarni, J. Nanophoton. 1 (2007) 012501.
[3] D. Felbacq, J. Nanophoton. 2 (2008) 020302.
[4] M. Svedendahl, S. Chen, A. Dmitriev, M. Kall, Nano Lett. 9 (2009) 4428.
[5] I. Abdulhalim, M. Zourob, A. Lakhtakia, Electromagnetics 28 (2008) 214.
[6] Y. Ding, Z.Q. Cao, Q.S. Shen, Opt. Quant. Electron. 35 (2003) 1091.
[7] Vladislav Lirtsman, Roy Ziblat, Michael Golosovsky, Dan Davidov, J. Appl. Phys. 98 (2005) 093507.
[8] Q. Cao, P. Lalanne, Phys. Rev. Lett. 88 (2002) 57403.
[9] W. Fan, S. Zhang, B. Minhas, K.J. Malloy, S.R.J. Brueck, Phys. Rev. Lett. 94 (2005) 33902.
[10] K.J.K. Koerkamp, S. Enoch, F.B. Segerink, N.F. Van Hulst, L. Kuipers, Phys. Rev. Lett. 92 (2004) 183901.
[11] J.Z. Zhang, C. Noguez, Plasmonics 3 (2008) 127.
[12] B.S. Passmore, D.G. Allen1, S.R. Vangala, W.D. Goodhue, D. Wasserman, E.A. Shaner, Opt. Express 17 (2009) 10223.
[13] Christophe Minot, Yanko Todorov, Damien Armand, Frédéric Garet, Jean-Louis Coutaz, Phys. Rev. B 80 (2009) 153410.
[14] J.M. Pitarke, V.M. Silkin, E.V. Chulkov, P.M. Echenique, Rep. Prog. Phys. 70 (2007) 1.
[15] A. Karabchevsky, O. Krasnykov, M. Auslender, B. Hadad, A. Goldner, I. Abdulhalim, Plasmonics 4 (2009) 1557.
[16] Jiri Homola, I. Koudela, S.S. Yee, Sensors Actuators A 54 (1999) 16.
[17] Amit Lahav, Atef Shalabney, I. Abdulhalim, J. Nanophoton. 3 (2009) 031501.
[18] A. Karabchevsky, O. Krasnykov, I. Abdulhalim, B. Hadad, A. Goldner, M. Auslender, S. Hava, Photon. Nanostruct. Fundam. Appl. 7 (2009) 170.